

Chapter 1 Climate in 2018

1.1 Global climate summary

- Extremely high summer temperatures were frequently observed worldwide, especially in the Northern Hemisphere during boreal summer, with records being set in Europe, East Asia and the southwestern USA.
- Extensive damage and numerous fatalities were caused by heavy rain from eastern to western Japan (June – July), in India (June – September), in Nigeria (July – September) and from northern to central parts of Eastern Africa (March – May), while significant agricultural losses were caused by droughts in and around northern Argentina (January – March) and in southeastern Australia (January – September).

Major extreme climate events¹ and weather-related disasters occurring in 2018 are shown in Figure 1.1-1 and Table 1.1-1.

Extremely high temperatures were frequently observed in many parts of the world ((1), (2), (5), (7), (10), (11), (12), (14), (16), (19), (21), (23), (25), (26) in Figure 1.1-1), even though the La Niña event that began in boreal fall 2017 continued to boreal spring 2018. Record temperatures were observed in Europe, East Asia and the southwestern USA in boreal summer ((14), (5), (21) in Figure 1.1-1), and seasonal mean temperatures for summer (June – August) were the highest on record in eastern Japan, Korea, China and the southwestern USA since 1946, 1973, 1961 and 1895, respectively (Japan Meteorological Agency, Korea Meteorological Administration, China Meteorological Administration, National Oceanic and Atmospheric Administration, USA; (5), (21) in Figure 1.1-1). An all-Japan record daily maximum temperature of 41.1°C was recorded at Kumagaya in Saitama Prefecture.

Contrasting extremes of high and low precipitation were frequently observed in southern and central Europe, respectively ((15) and (13) in Figure 1.1-1). Extremely high precipitation amounts were observed from northeastern to southern parts of the USA (February, May, August – December; (20) in Figure 1.1-1), and seasonal precipitation amounts in fall (September – November) were the highest, second highest and third highest in the southern, northeastern and northern Midwest USA, respectively (National Oceanic and Atmospheric Administration, USA).

Climate extremes caused immense damage worldwide. Japan experienced unprecedentedly heavy rain from its western part to the Tokai region around early July due to a stationary Baiu front and Typhoon Prapiroon, which resulted in 224 fatalities (Cabinet Office of Japan, as of 9 October 2018; (6) in Figure 1.1-1). Heavy rain caused more than 1,500 fatalities in India (June – September) and more than 300 fatalities in Nigeria (July – September) ((9), (17) in Figure 1.1-1). From northern to central parts of Eastern Africa, intermittent heavy rain from March to May and Tropical Storm Sagar in May resulted in more than 500 fatalities ((18) in Figure 1.1-1). Extreme drought conditions in southeastern Australia (January – September; (27) in Figure 1.1-1) made 2018 the worst year in terms of farm cash income since 1978, prompting comparisons to the extreme drought conditions of 2002 – 2003. Total precipitation in New South Wales, Australia, from January to September was the third lowest for the period since 1900 (Bureau of Meteorology, Australia).

¹ Extreme climate events are defined by anomalies or ratios to climatological normals. Normals represent mean climate conditions at given sites, and are currently based on a 30-year mean covering the period from 1981-2010.

Annual mean temperatures were above normal in most parts of the world, and were very high from Alaska to northwestern Siberia, in the southern part of East Asia, from Micronesia to the central part of Southeast Asia, in the western part of South Asia, from Europe to the Middle East, in and around the southern part of Eastern Africa, from western to southeastern parts of the USA, from Central America to the eastern part of South America, and in Australia. Annual mean temperatures were below normal from eastern Canada to the northern USA, and were very low in and around the northeastern part of Central Asia (Figure 1.1-2).

Annual precipitation amounts were above normal from Mongolia to northern China, from eastern to central parts of Central Asia, from the northwestern part of the Middle East to the eastern part of Northern Africa, from southern Europe to the northwestern part of Northern Africa, and from northeastern to southern parts of the USA, and were below normal in the western part of Central Asia, from the northwestern part of South Asia to the southern part of the Middle East, and in southeastern Australia (Figure 1.1-3).

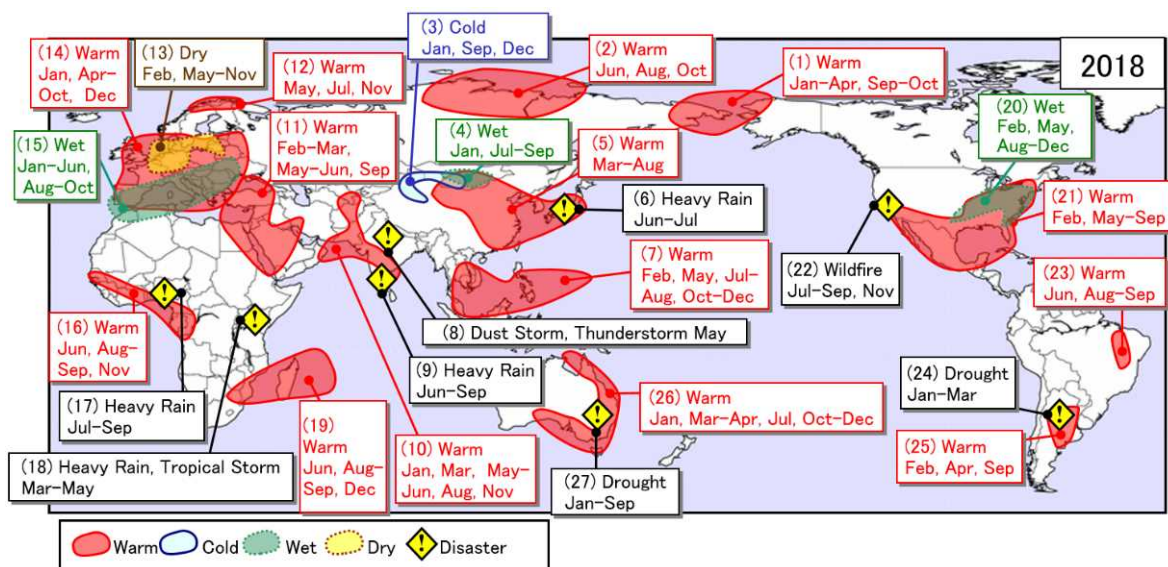


Figure 1.1-1 Major extreme events and weather-related disasters observed in 2018²

Schematic representation of major extreme climatic events and weather-related disasters occurring during the year.

“Warm”, “Cold”, “Wet” and “Dry” indicate that monthly extreme events occurred three times or more during the year in these regions. JMA defines an extreme climate event as a phenomenon likely to happen only once every 30 years.

Data and information on disasters are based on official reports of the United Nations and national governments and databases of research institutes (EM-DAT).

EM-DAT: The Emergency Events Database - Université Catholique de Louvain (UCL) - CRED, D. Guha-Sapir - www.emdat.be, Brussels, Belgium.

² Annual distribution maps for major extreme climatic events and weather-related disasters after 2008 are provided at JMA’s website.

<https://ds.data.jma.go.jp/tcc/tcc/products/climate/annual/index.html>

Table 1.1-1 Major extreme events and weather-related disasters occurring in 2018

No.	Event
(1)	Warm: from western Alaska to the eastern part of Eastern Siberia (January – April, September – October)
(2)	Warm: from the northwestern part of Eastern Siberia to the northwestern part of Central Siberia (June, August, October)
(3)	Cold: from southwestern Mongolia to northwestern China (January, September, December)
(4)	Wet: in and around central Mongolia (January, July – September)
(5)	Warm: from northern Japan to northwestern China (March – August)
(6)	Heavy Rain: from eastern to western Japan (June – July)
(7)	Warm: from northwestern Micronesia to the northwestern part of Southeast Asia (February, May, July – August, October – December)
(8)	Dust Storm and Thunderstorm: northern India (May)
(9)	Heavy Rain: India (June – September)
(10)	Warm: from the southern part of Central Asia to the southeastern part of South Asia (January, March, May – June, August, November)
(11)	Warm: in and around Middle East (February – March, May – June, September)
(12)	Warm: the northern Scandinavian Peninsula (May, July, November)
(13)	Dry: in and around central Europe (February, May – November)
(14)	Warm: from central to southern Europe (January, April – October, December)
(15)	Wet: from southern Europe to the northwestern part of Northern Africa (January – June, August – October)
(16)	Warm: from the western part of Western Africa to the northwestern part of Middle Africa (June, August – September, November)
(17)	Heavy Rain: Nigeria (July – September)
(18)	Heavy Rain and Tropical Storm: from the northern to central parts of Eastern Africa (March – May)
(19)	Warm: from Mauritius to northwestern South Africa (June, August – September, December)
(20)	Wet: from the northeastern to southern USA (February, May, August – December)
(21)	Warm: from the southern part of North America to the central part of Central America (February, May – September)
(22)	Wildfire: the western USA (July – September, November)
(23)	Warm: northeastern Brazil (June, August – September)
(24)	Drought: in and around northern Argentina (January – March)
(25)	Warm: from northern to central Argentina (February, April, September)
(26)	Warm: from eastern to southern Australia (January, March – April, July, October – December)
(27)	Drought: southeastern Australia (January – September)

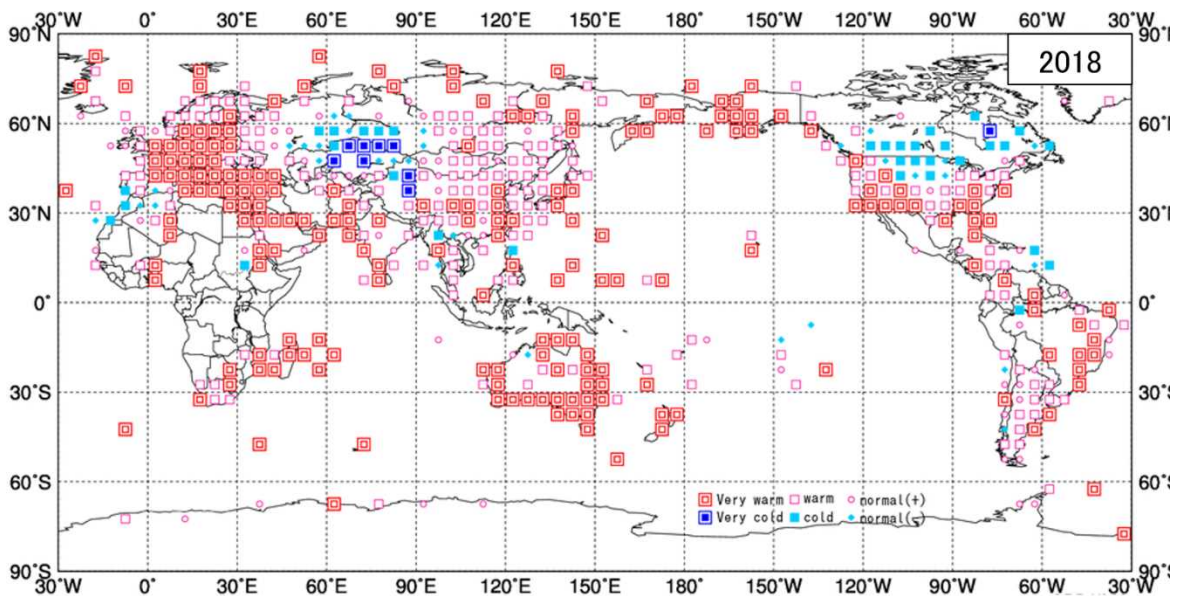


Figure 1.1-2 Annual mean temperature anomalies in 2018³

Categories are defined by the annual mean temperature anomaly against the normal divided by its standard deviation and averaged in $5^\circ \times 5^\circ$ grid boxes. Red/blue marks indicate values above/below the normal calculated for the period from 1981 to 2010. The thresholds of each category are -1.28 , -0.44 , 0 , $+0.44$ and $+1.28$ ⁴. Areas over land without graphical marks are those where observation data are insufficient or normal data are unavailable.

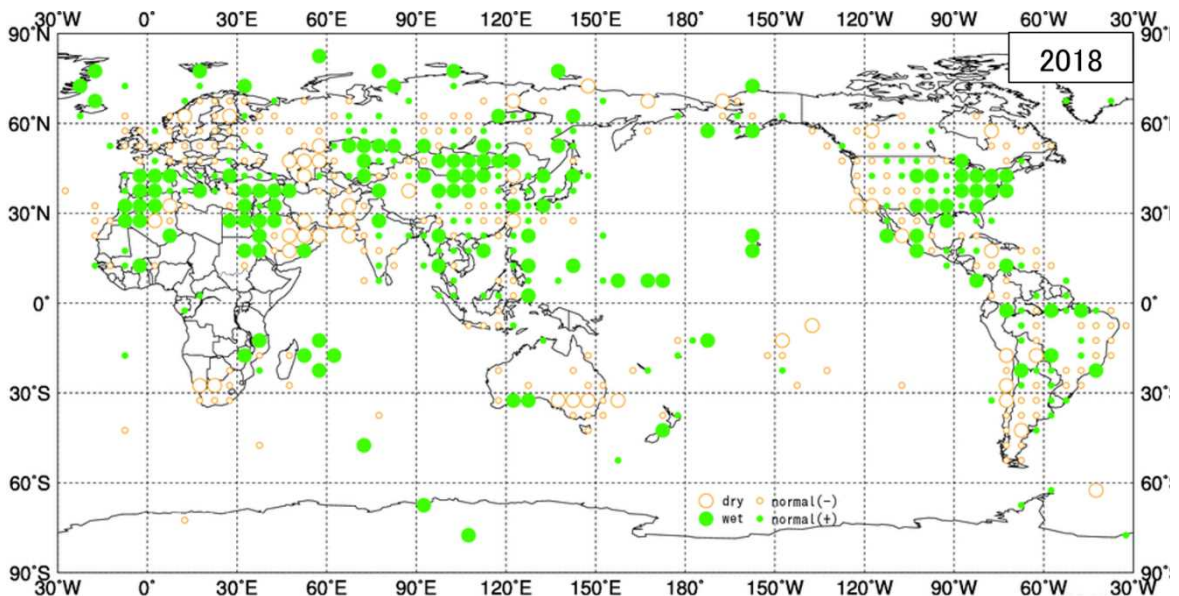


Figure 1.1-3 Annual total precipitation amount ratios in 2018

Categories are defined by the annual precipitation ratio to the normal averaged in $5^\circ \times 5^\circ$ grid boxes. Green/yellow marks indicate values above/below the thresholds. The thresholds of each category are 70, 100 and 120% of the normal calculated for the period from 1981 to 2010. Areas over land without graphical marks are those where observation data are insufficient or normal data are unavailable.

³ Distribution maps for normalized annual mean temperature anomaly and precipitation amount ratio to normal after 2008 are provided at JMA's website.

<https://ds.data.jma.go.jp/tcc/tcc/products/climate/annual/index.html>

⁴ In normal distribution, values of 1.28 and 0.44 correspond to occurrence probabilities of less than 10 and 33.3%, respectively.

1.2 Climate in Japan⁵

- In winter (Dec. 2017 – Feb. 2018), seasonal mean temperatures were below normal nationwide, with heavy snowfall on the Sea of Japan side of eastern Japan and elsewhere.
- In spring and summer, record-high seasonal mean temperatures were observed in eastern and western Japan.
- In early July, western Japan sustained significant damage from several days of unprecedentedly heavy rain.
- Typhoons Jebi and Trami made landfall on or approached Japan, causing storms and high tides.

1.2.1 Annual characteristics

The annual climate anomaly/ratio for Japan in 2018 is shown in Figure 1.2-1.

- Annual mean temperatures: above normal in nationwide, especially in eastern Japan
- Annual precipitation amounts: above normal nationwide except on the Pacific side of eastern Japan, especially on the Sea of Japan of northern Japan and on the Pacific side of western Japan
- Annual sunshine durations: above normal nationwide except in northern Japan

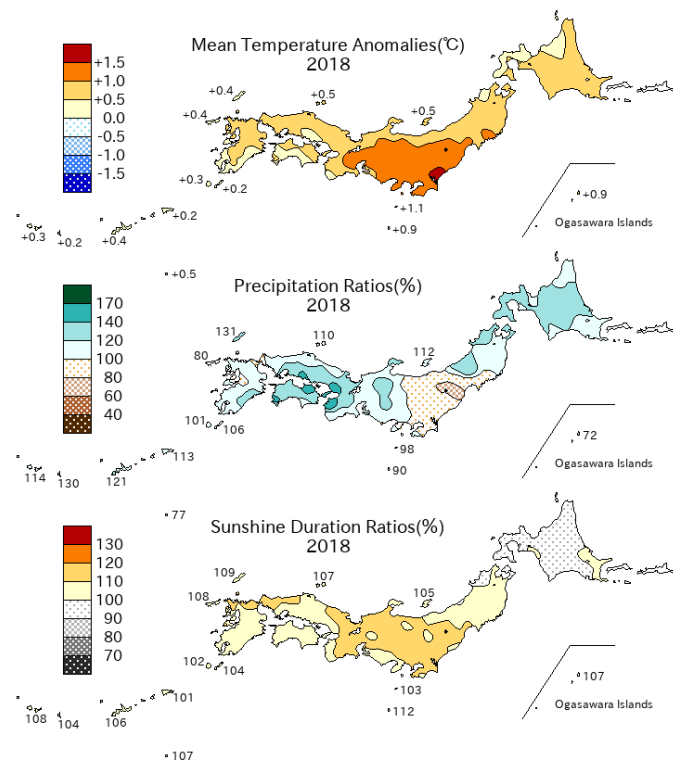


Figure 1.2-1 Annual climate anomaly/ratio for Japan in 2018

The base period for the normal is 1981 – 2010.

⁵ The term *significantly above normal* is used for cases in which observed mean temperatures or precipitation amounts exceed the 90th percentile for the base period (1981 – 2010), and *significantly below normal* is used when the corresponding figures fall below the 10th percentile.

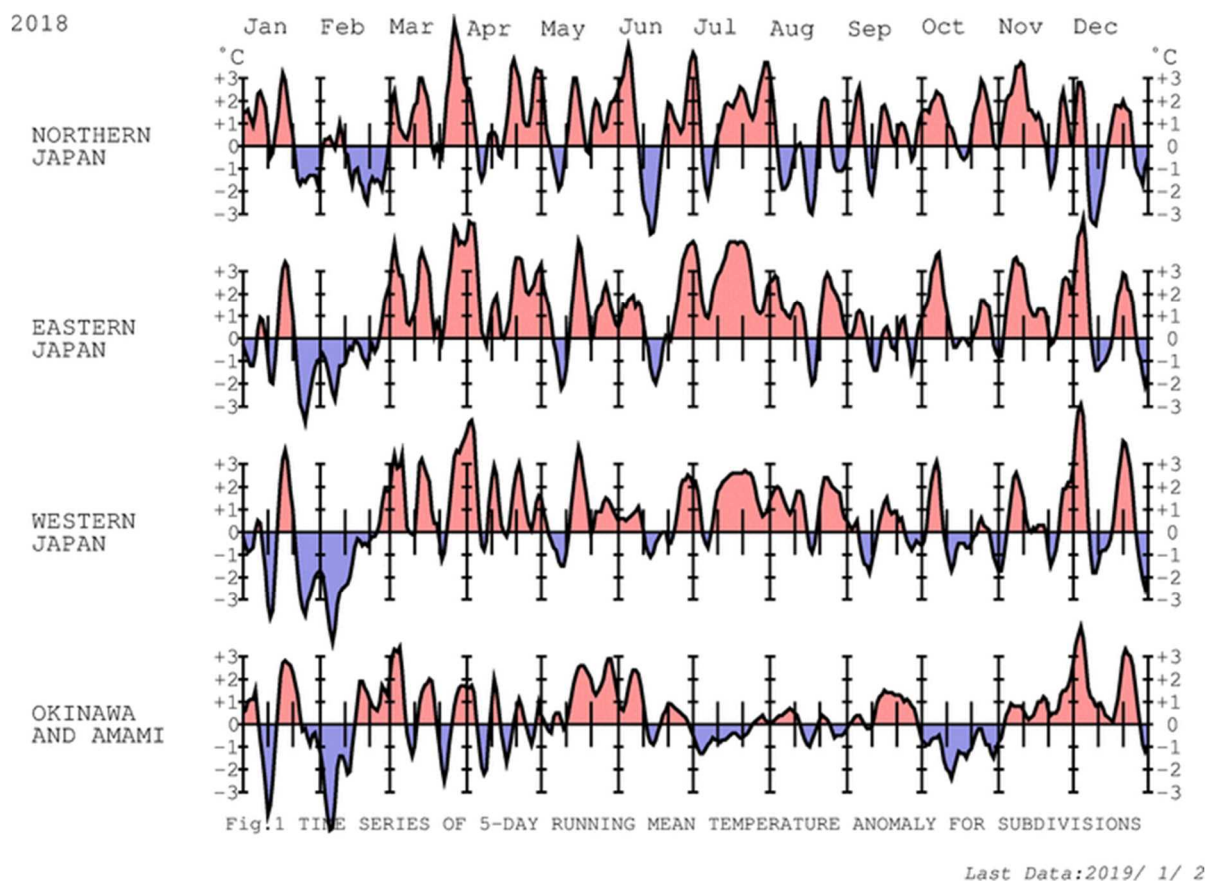


Figure 1.2-2 Five-day running mean temperature anomaly for divisions (January – December 2018)
The base period for the normal is 1981 – 2010.

1.2.2 Seasonal characteristics

Five-day running mean temperature anomalies for different divisions (January – December 2018) are shown in Figure 1.2-2, and seasonal anomalies/ratios for Japan in 2018 are shown in Figure 1.2-3. Numbers of observatories reporting record monthly and annual mean temperatures, precipitation amounts and sunshine durations (2018) are shown in Table 1.2-1.

(1) Winter (December 2017 – February 2018)

- Mean temperatures: below normal nationwide
- Precipitation amounts: significantly above normal on the Sea of Japan side of eastern and western Japan, above normal on the Sea of Japan side of northern Japan, below normal on the Pacific side of eastern Japan, on the Sea of Japan side of western Japan, and in Okinawa/Amami, near normal on the Pacific side of northern and western Japan
- Sunshine durations: significantly above normal on the Pacific side of eastern Japan, above normal on the Pacific side of western Japan and in Okinawa/Amami, near normal on the Pacific side of northern Japan, on the Sea of Japan side of eastern and western Japan

In association with a strong winter monsoon, seasonal mean temperatures were below normal nationwide. In particular, the value for western Japan was the lowest for 32 years at 1.2°C below the normal. On the Sea of Japan side from northern to western Japan, heavy clouds flowing in quickly from the Sea of Japan brought heavy snowfall and traffic disruption on the eastern side. The maximum snow depth in Fukui exceeded 140 cm for the first time in 37 years (147 cm).

(2) Spring (March – May 2018)

- Mean temperatures: significantly above normal nation wide
- Precipitation amounts: above normal from northern to western Japan, especially on the Sea of Japan side of northern and eastern Japan, significantly below normal in Okinawa/Amami
- Sunshine durations: significantly above normal on the Pacific side of eastern Japan and in western Japan and Okinawa/Amami, above normal on the Sea of Japan side of eastern Japan, near normal in northern Japan

Seasonal mean temperatures were significantly above normal nationwide as a result of warm air masses over Japan throughout the period. The value for eastern Japan was the highest since records began in 1946, at 2.0°C over the normal. Sunny conditions and high pressure prevailed from eastern Japan to Okinawa/Amami, while northern to western parts of Japan experienced heavy rain in association with the passage of low-pressure areas containing moist air from the south. Seasonal sunshine durations were significantly above normal on the Pacific side of eastern Japan, in western Japan and in Okinawa/Amami. Seasonal precipitation amounts were significantly above normal on the Sea of Japan side of northern Japan and eastern parts of the country, and were significantly below normal in Okinawa/ Amami.

(3) Summer (June – August 2018)

- Mean temperatures: significant above normal in eastern and western Japan, above normal in northern Japan, near normal in Okinawa/Amami
- Precipitation amounts: significantly above normal on the Sea of Japan side of northern Japan, on the Pacific side of western Japan, and in Okinawa/Amami, above normal on the Pacific side of northern Japan, near normal in eastern Japan and on the Sea of Japan side of western Japan
- Sunshine durations: below normal on the Sea of Japan side of northern Japan and in Okinawa/Amami, significantly above normal in eastern Japan and on the Sea of Japan side of western Japan, near normal on the Pacific side of northern Japan

In early July, several days of record rainfall were observed in western Japan due to the influence of an active Baiu front, causing serious damage including landslides and floods. From mid-July onward, very hot conditions continued in eastern and western Japan due to the presence of a pronounced Subtropical High and Tibetan High over the country. The rainy Baiu season ended significantly earlier than usual in many regions, and very hot conditions continued in eastern and western Japan. On July 23, Japan's all-time high temperature of 41.1°C was recorded at Kumagaya in Saitama Prefecture. The seasonal mean temperature in eastern Japan was the highest for summer since 1946, at 1.7°C above the normal. At 48 of the country's 153 meteorological stations, the seasonal mean temperature for summer was highest or joint-highest on record. Seasonal precipitation amounts were significantly above normal on the Sea of Japan side of northern Japan and from eastern Japan to Okinawa/Amami due to the influence of stationary fronts or typhoons. In Okinawa/Amami, seasonal precipitation amounts were the highest since 1946.

(4) Autumn (September – November 2018)

- Mean temperatures: above normal in eastern and western Japan, near normal in northern and Japan and Okinawa/Amami
- Precipitation amounts: above normal from eastern Japan to Okinawa/Amami, below normal in northern Japan
- Sunshine durations: below normal in eastern Japan and on the Sea of Japan side of western Japan, above normal in northern Japan and Okinawa /Amami, near normal on the Pacific side of western Japan

Seasonal mean temperatures were above normal in northern and eastern Japan because stronger-than-normal high-pressure areas to the east of the country hindered the flow of northerly cold air over these regions. Seasonal precipitation amounts were above normal from eastern Japan to Okinawa/Amami due to the influence of an active stationary front and typhoon activity. In early September, the strong Typhoon Jebi made landfall on the southern part of Tokushima before heading north to the Kinki region. In late September Typhoon Trami approached the Okinawa region and made landfall near Tanabe in Wakayama Prefecture before moving from western to northern Japan, bringing storms, heavy rain, storm surges and high waves to wide areas.

(5) Early Winter (December 2018)

Above-normal temperatures prevailed nationwide except in northern Japan. However, heavy snowfall and snowstorms were observed on the Sea of Japan side of the country in late December due to a strong winter monsoon.

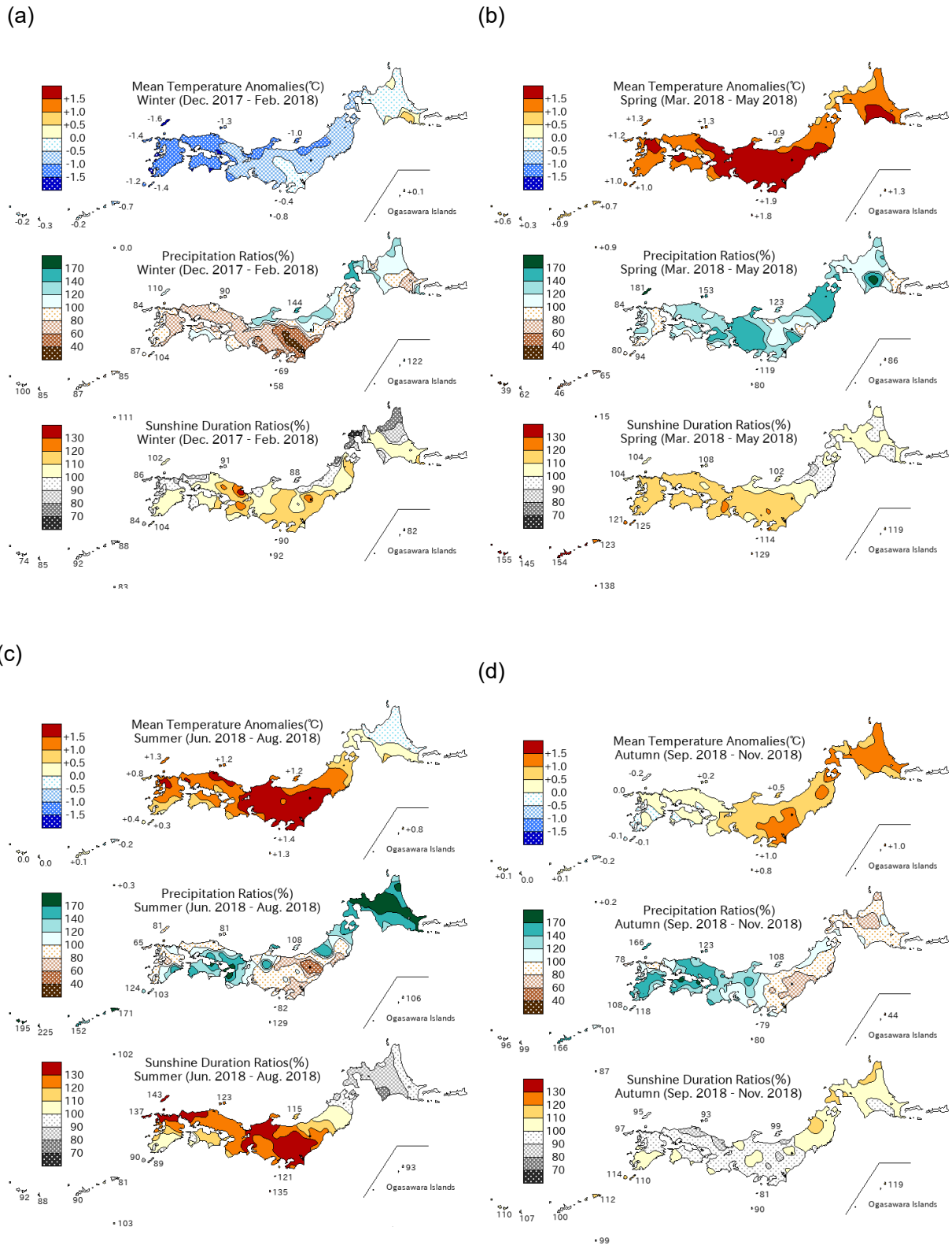


Figure 1.2-3 Seasonal anomalies/ratios for Japan in 2018
(a) Winter (December 2017 to February 2018), (b) spring (March to May 2018), (c) summer (June to August 2018), (d) autumn (September to November 2018). The base period for the normal is 1981 – 2010.

Table 1.2-1 Number of observatories reporting record(include tie record) monthly and annual mean temperatures, precipitation amounts and sunshine durations (2018)

From 153 surface meteorological stations across Japan.

	Temperature		Precipitation amount		Sunshine duration	
	Highest	Lowest	Heaviest	Lightest	Longest	Shortest
January						
February				4	3	
March	60		9		29	
April	21			2	2	
May	1		1	1	1	
June			1	4	2	
July	53		1		5	1
August	12		2	2	1	
September	1		7	6		
October	4					4
November				6	4	
December	1		1	1		6
year	29		2		4	

1.3 Atmospheric circulation and oceanographic conditions⁶

- In winter 2017/2018, tropical convection was enhanced from the Indochina Peninsula to seas east of the Philippines due to La Niña conditions. The subtropical and subpolar jet stream meandered southward over Japan, resulting in strong cold-air-mass flow over the country.
- In summer 2018, as a result of enhanced convection over and around the Philippines as well as the significant northward meandering of the subtropical jet stream in the vicinity of Japan, the expansion of both the North Pacific Subtropical High and the Tibetan High to mainland Japan was stronger than normal. The record heatwave observed in eastern and western Japan is attributed to these conditions.

Monitoring of atmospheric and oceanographic conditions (e.g., upper air flow, tropical convective activity, sea surface temperatures (SSTs) and the Asian monsoon) is key to understanding the causes of extreme weather events⁷. This section briefly outlines the characteristics of atmospheric circulation and oceanographic conditions seen in 2018.

1.3.1 Characteristics of individual seasons⁸

(1) Winter (December 2017 – February 2018)

La Niña conditions continued in the equatorial Pacific from autumn 2017 onward (see Section 2.6.1), with positive SST anomalies in the western part and negative values from central to eastern parts (Figure 1.3-1 (a)). Tropical convection activity was enhanced from the Indochina Peninsula to seas east of the Philippines, and was suppressed from west of the dateline to the central part of the equatorial Pacific (Figure 1.3-1 (b)). In the lower troposphere of the tropical region, cyclonic circulation anomalies straddling the equator were seen from the Indian Ocean to the Maritime Continent (Figure 1.3-1 (c)).

Positive anomalies in the 500-hPa height field were seen in and around the North Pole, and negative height anomalies were seen over Europe. The polar vortex split into East Siberian and North American parts, with respective wave trains clearly observed over southern and northern Eurasia (Figure 1.3-1 (d)). The sea level pressure (SLP) field indicates that the Siberian High was stronger than normal in general and extended northwestward, and that the Aleutian Low was shifted westward and stronger than normal over and around the Kamchatka Peninsula (Figure 1.3-1 (e)). Temperatures at 850 hPa were above normal over the Arctic Ocean and below normal over East Asia, the northern part of North America and Europe (Figure 1.3-1 (f)).

⁶ See the Glossary for terms relating to sea surface temperature variations, monsoon and Arctic Oscillation.

⁷ The main charts used for monitoring of atmospheric circulation and oceanographic conditions are: sea surface temperature (SST) maps representing SST distribution for monitoring of oceanographic variability elements such as El Niño/La Niña phenomena; outgoing longwave radiation (OLR) maps representing the strength of longwave radiation from the earth's surface under clear sky conditions into space or from the top of clouds under cloudy conditions into space for monitoring of convective activity; 850-hPa stream function maps representing air flow in the lower troposphere for monitoring of atmospheric circulation variability elements such as the Pacific High and the monsoon trough associated with the Asian summer monsoon; 500-hPa height maps representing air flow at a height of approximately 5,000 meters for monitoring of atmospheric circulation variability elements such as westerly jet streams and the Arctic Oscillation; sea level pressure maps representing air flow and pressure systems on the earth's surface for monitoring of the Pacific High, the Siberian High, the Arctic Oscillation and other phenomena; 850-hPa temperature maps representing air temperature at a height of approximately 1,500 meters; and temperature calculated from thickness in the troposphere for monitoring of mean temperature of the troposphere.

⁸ JMA publishes Monthly Highlights on the Climate System including information on the characteristics of climatic anomalies and extreme events around the world, atmospheric circulation and oceanographic conditions. It can be found at <https://ds.data.jma.go.jp/tcc/tcc/products/clisys/highlights/index.html>.

With enhanced convection over the Maritime Continent and southward expansion of the polar vortex to eastern Siberia, the subtropical and subpolar jet stream meandered southward over Japan, resulting in cold air-mass flow over the country. This is a possible cause of the tendency for the presence of cold air in areas near Japan.

(2) Spring (March – May 2018)

Ongoing remarkable positive SST anomalies in the western part of the equatorial Pacific and negative values from central to eastern parts were observed, despite the termination of the La Niña event in spring 2018. Remarkably positive SST anomalies were observed from the area east of the Philippines to the western coast of Central America in the tropical North Pacific, and remarkably negative SST anomalies were observed in the eastern part of the tropical South Pacific (Figure 1.3-2 (a)). Tropical convection was enhanced from Eastern Africa to the central Indian Ocean and from Micronesia to Hawaii, and was suppressed from the South China Sea to seas east of Japan and in the central-to-eastern equatorial Pacific (Figure 1.3-2 (b)). In the lower troposphere of the tropical region, anti-cyclonic circulation anomalies were seen over the central-to-eastern Pacific, and cyclonic circulation anomalies were seen over the east of the Philippines (Figure 1.3-2 (c)).

In the 500-hPa height field, wave trains were seen from the North Atlantic to northern Eurasia along the subpolar jet stream, with positive anomalies over northern Europe and the northeastern part of East Asia, and negative anomalies from western Russia to western Siberia (Figure 1.3-2 (d)). Positive SLP anomalies were seen over the central part of North America and northern Europe, and negative SLP anomalies were seen from the northeastern part of the North Atlantic to western Europe and Siberia. Positive SLP anomalies extended zonally over the mid-latitudes from Japan to the North Pacific, and the subtropical high was stronger than normal over the North Pacific and the North Atlantic (Figure 1.3-2 (e)). Temperatures at the 850-hPa level were above normal over the western USA, southern Europe and the mid-latitudes from East Asia to the North Pacific, and were below normal over the northeastern part of North America and from western Russia to western Siberia (Figure 1.3-2 (f)).

(3) Summer (June – August 2018)

SST anomalies were remarkably positive in the western part of the equatorial Pacific and remarkably negative in the Indian Ocean south of Java. The North Atlantic tripole pattern exhibited remarkably positive SST anomalies in the mid-latitudes and remarkably negative values south of Greenland and in the eastern part of the tropical region (Figure 1.3-3 (a)). Tropical convection was enhanced from the Philippines to the 10 – 20°N latitude band in the North Pacific, and was suppressed over the Indian Ocean and the central part of the South Pacific (Figure 1.3-3 (b)). In the lower troposphere over the tropical region, cyclonic circulation anomalies were seen from the northern part of the South China Sea to seas east of the Philippines, indicating a stronger-than-normal monsoon trough over Southeast Asia (Figure 1.3-3 (c)).

In the 500-hPa height field, the polar vortex in the Northern Hemisphere was shifted toward North America. Positive anomalies in the 500-hPa height field were generally distributed over the mid-latitudes, and were seen over the seas south of Alaska, the eastern part of North America, northern Europe, from Central to Eastern Siberia and over the northeastern part of East Asia. Negative anomalies in the 500-hPa height field were seen over the Mediterranean Sea and from the South China Sea to seas south of Japan (Figure 1.3-3 (d)). Negative SLP anomalies were seen

in and around Greenland, and positive SLP anomalies were seen over the mid-latitudes of the North Pacific and the North Atlantic. The extension of the North Pacific Subtropical High (NPSH) toward mainland Japan was stronger than normal (Figure 1.3-3 (e)). Temperatures at 850 hPa were above normal over seas south of Alaska, the eastern part of North America, northern Europe, from Central to Eastern Siberia, and over the eastern part of East Asia, and below normal over northern Canada and the Sea of Okhotsk (Figure 1.3-3 (f)).

In summer, as the result of enhanced convective activity over and around the Philippines as well as the significant meandering of the subtropical jet stream in the vicinity of Japan, the expansion of both the NPSH and the Tibetan High to mainland Japan was stronger than normal. The record-breaking extreme heatwave in eastern and western Japan is attributed to these conditions (see Topics I).

(4) Autumn (September – November 2018)

Positive SST anomalies were observed over most of the equatorial Pacific, and remarkably positive anomalies were observed in western parts of the tropical region. El Niño conditions were considered present in autumn. In the Indian Ocean, remarkably negative SST anomalies were observed near the southwestern coast of Australia, and the North Atlantic SST anomaly tripole pattern remained following the anomaly observed in summer 2018 (Figures 1.3-3 (a) and 1.3-4 (a)). Tropical convection was enhanced over seas east of New Guinea, over the latitudinal bands of 10°N in central to eastern areas of the Pacific and from Western Africa to the Middle East, and was suppressed over the eastern Indian Ocean and from the South China Sea to seas east of the Philippines (Figure 1.3-4 (b)). In the lower troposphere of the tropical region, anticyclonic circulation anomalies straddling the equator were seen from the Indian Ocean to the Maritime Continent, and cyclonic circulation anomalies straddling the equator were seen over the Pacific (Figure 1.3-4 (c)).

Positive anomalies in the 500-hPa height field were clearly seen in and around Alaska and over northern Europe, and negative values were seen from central Canada to seas west of the UK and in and around China (Figure 1.3-4 (d)). Positive SLP anomalies were seen from northern Europe to Central Asia and from Alaska to Canada, and negative values were seen over Western Siberia (Figure 1.3-4 (e)). Temperatures at 850 hPa were above normal in and around Alaska and Europe, and below normal over the eastern part of North America (Figure 1.3-4 (f)).

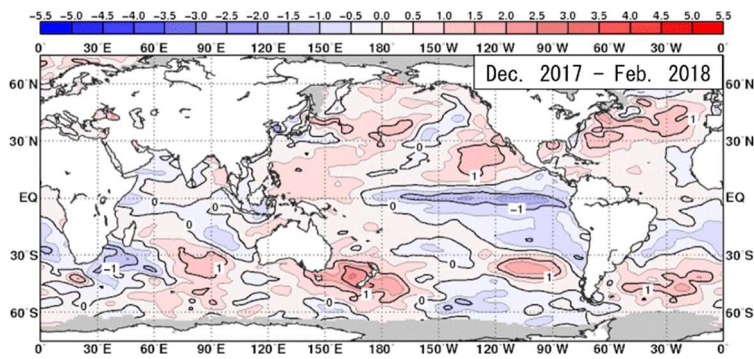


Figure 1.3-1 (a) Three-month mean sea surface temperature (SST) anomaly (December 2017 – February 2018). The contour interval is 0.5°C. Sea ice coverage areas are shaded in gray. The base period for the normal is 1981 – 2010.

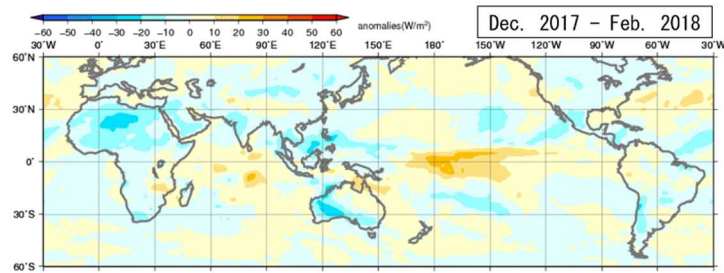


Figure 1.3-1 (b) Three-month mean outgoing longwave radiation (OLR) anomaly (December 2017 – February 2018). The base period for the normal is 1981 – 2010. Negative (cold color) and positive (warm color) OLR anomalies show enhanced and suppressed convection, respectively, compared to the normal.

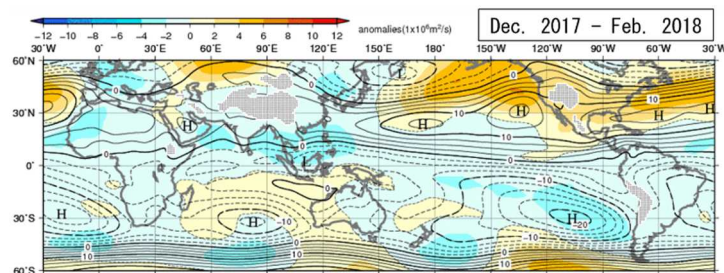


Figure 1.3-1 (c) Three-month mean 850-hPa stream function and anomaly (December 2017 – February 2018). The contour interval is $2.5 \times 10^6 \text{ m}^2 \text{ per s}$. The base period for the normal is 1981 – 2010. “H” and “L” denote high- and low-pressure systems, respectively.

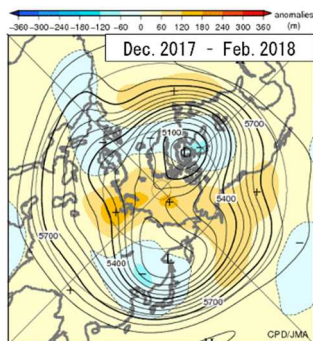


Figure 1.3-1 (d) Three-month mean 500-hPa height and anomaly in the Northern Hemisphere (December 2017 – February 2018). Contours show 500-hPa height at intervals of 60 m, and shading indicates height anomalies. The base period for the normal is 1981 – 2010. “H” and “L” denote high- and low-pressure systems, respectively.

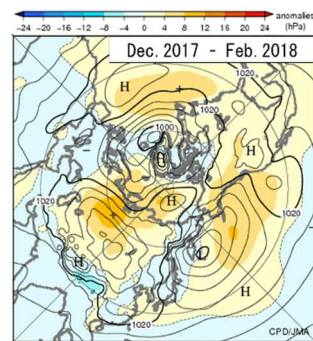


Figure 1.3-1 (e) Three-month mean sea level pressure and anomaly in the Northern Hemisphere (December 2017 – February 2018). Contours show sea level pressure at intervals of 4 hPa, and shading indicates sea level pressure anomalies. The base period for the normal is 1981 – 2010. “H” and “L” denote high- and low-pressure systems, respectively.

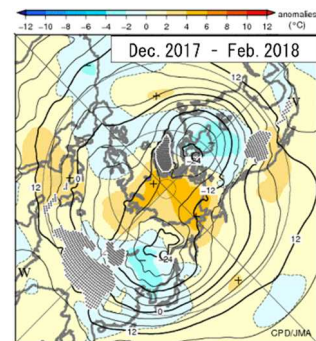


Figure 1.3-1 (f) Three-month mean 850-hPa temperature and anomaly in the Northern Hemisphere (December 2017 – February 2018). Contours show temperature at intervals of 4 degree C, and shading indicates temperature anomalies. The base period for the normal is 1981 – 2010. “W” and “C” denote warm and cold conditions, respectively.

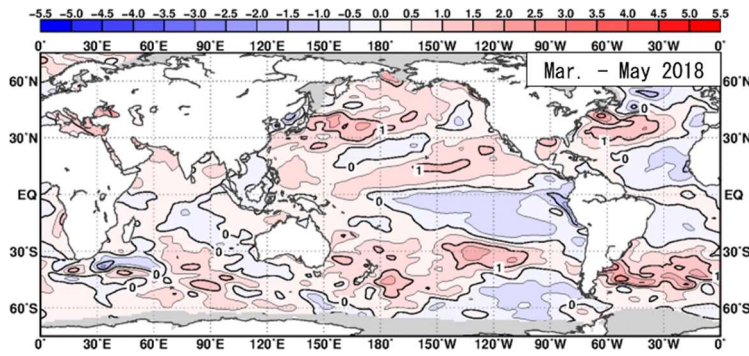


Figure 1.3-2 (a) Three-month mean sea surface temperature (SST) anomaly (March – May 2018)
As per Figure 1.3-1 (a), but for March – May 2018.

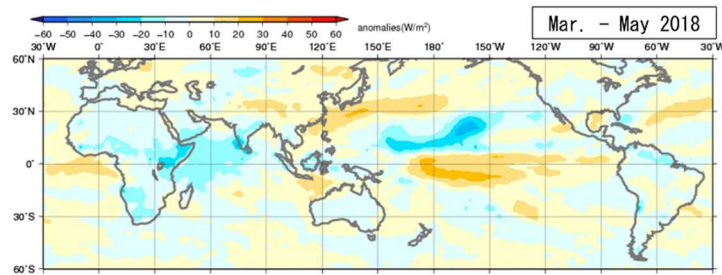


Figure 1.3-2 (b) Three-month mean outgoing longwave radiation (OLR) anomaly (March – May 2018)
As per Figure 1.3-1 (b), but for March – May 2018.

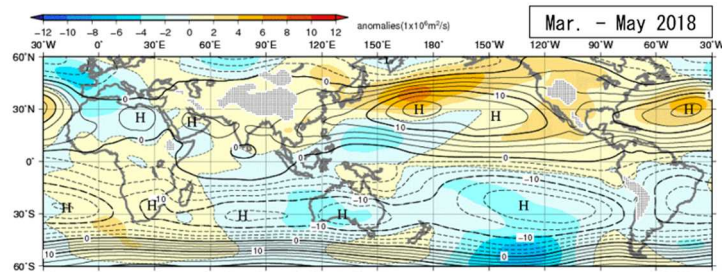


Figure 1.3-2 (c) Three-month mean 850-hPa stream function and anomaly (March – May 2018)
As per Figure 1.3-1 (c), but for March – May 2018.

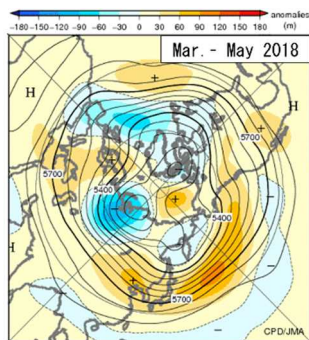


Figure 1.3-2 (d) Three-month mean 500-hPa height and anomaly in the Northern Hemisphere (March – May 2018)
As per Figure 1.3-1 (d), but for March – May 2018.

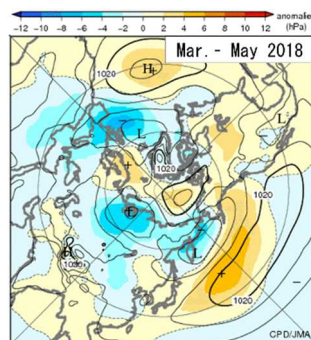


Figure 1.3-2 (e) Three-month mean sea level pressure and anomaly in the Northern Hemisphere (March – May 2018)
As per Figure 1.3-1 (e), but for March – May 2018.

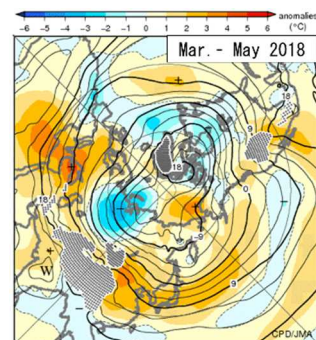


Figure 1.3-2 (f) Three-month mean 850-hPa temperature and anomaly in the Northern Hemisphere (March – May 2018)
As per Figure 1.3-1 (f), but for March – May 2018.
Contour interval is 3 degree C.

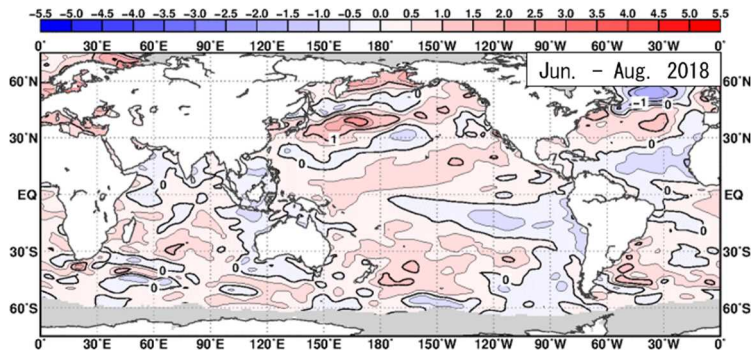


Figure 1.3-3 (a) Three-month mean sea surface temperature (SST) anomaly (June – August 2018)
As per Figure 1.3-1 (a), but for June – August 2018.

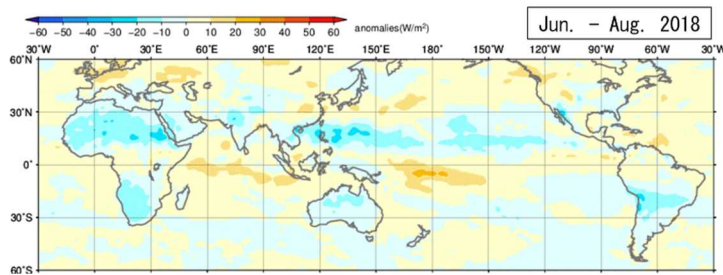


Figure 1.3-3 (b) Three-month mean outgoing longwave radiation (OLR) anomaly (June – August 2018)
As per Figure 1.3-1 (b), but for June – August 2018.

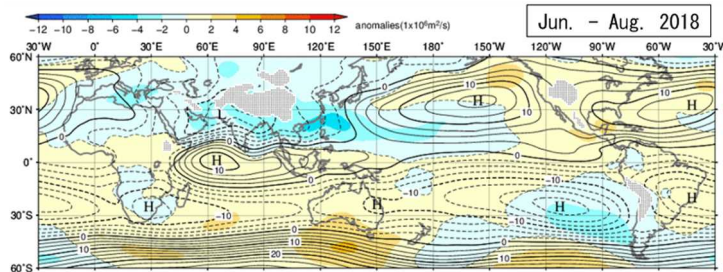


Figure 1.3-3 (c) Three-month mean 850-hPa stream function and anomaly (June – August 2018)
As per Figure 1.3-1 (c), but for June – August 2018.

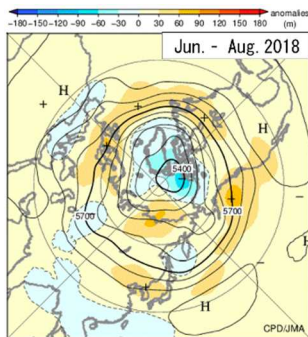


Figure 1.3-3 (d) Three-month mean 500-hPa height and anomaly in the Northern Hemisphere (June – August 2018)
As per Figure 1.3-1 (d), but for June – August 2018.

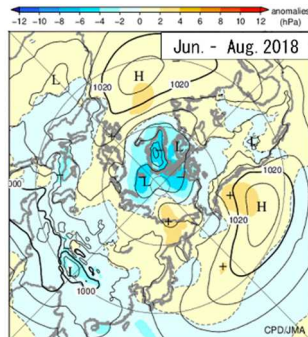


Figure 1.3-3 (e) Three-month mean sea level pressure and anomaly in the Northern Hemisphere (June – August 2018)
As per Figure 1.3-1 (e), but for June – August 2018.

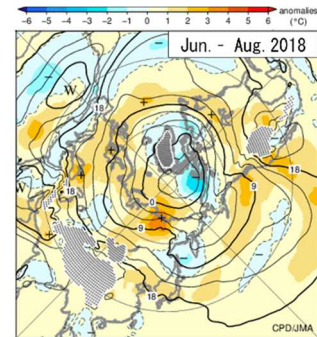


Figure 1.3-3 (f) Three-month mean 850-hPa temperature and anomaly in the Northern Hemisphere (June – August 2018)
As per Figure 1.3-1 (f), but for June – August 2018.
Contour interval is 3 degree C.

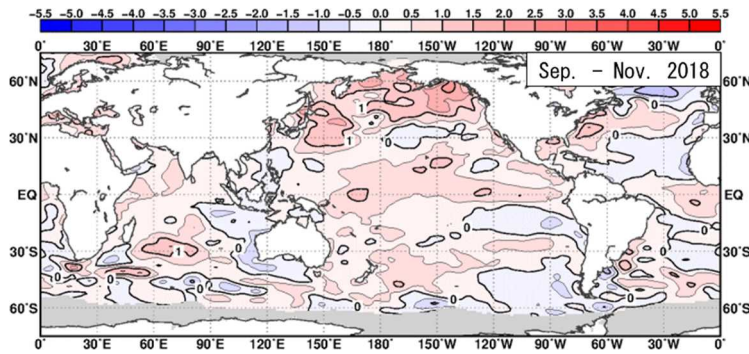


Figure 1.3-4 (a) Three-month mean sea surface temperature (SST) anomaly (September – November 2018)
As per Figure 1.3-1 (a), but for September – November 2018.

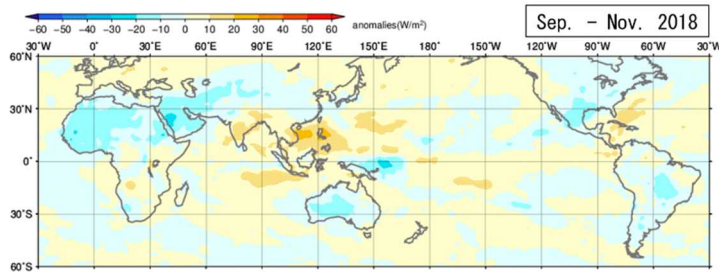


Figure 1.3-4 (b) Three-month mean outgoing longwave radiation (OLR) anomaly (September – November 2018)
As per Figure 1.3-1 (b), but for September – November 2018.

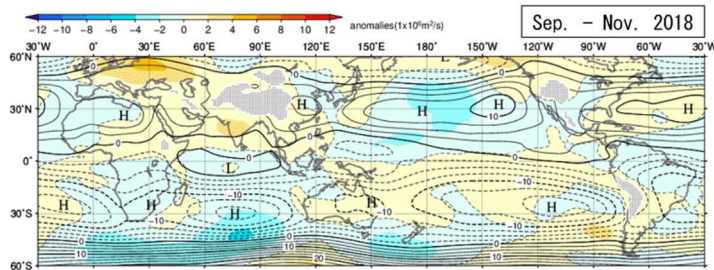


Figure 1.3-4 (c) Three-month mean 850-hPa stream function and anomaly (September – November 2018)
As per Figure 1.3-1 (c), but for September – November 2018.

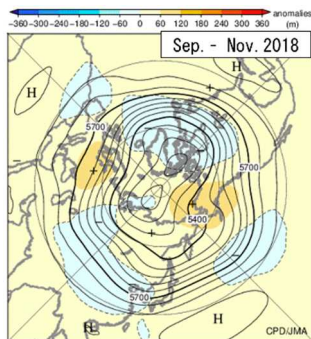


Figure 1.3-4 (d) Three-month mean 500-hPa height and anomaly in the Northern Hemisphere (September – November 2018)
As per Figure 1.3-1 (d), but for September – November 2018.

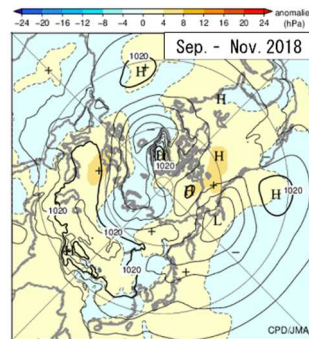


Figure 1.3-4 (e) Three-month mean sea level pressure and anomaly in the Northern Hemisphere (September – November 2018)
As per Figure 1.3-1 (e), but for September – November 2018.

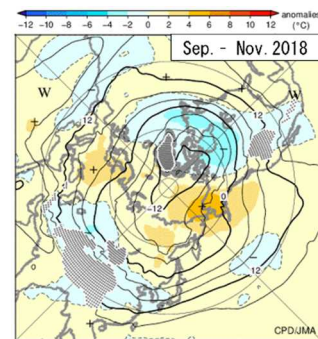


Figure 1.3-4 (f) Three-month mean 850-hPa temperature and anomaly in the Northern Hemisphere (September – November 2018)
As per Figure 1.3-1 (f), but for September – November 2018.

1.3.2 Global average temperature in the troposphere

The global average temperature in the troposphere peaked in spring 2016 and remained higher than normal until 2018 (Figure 1.3-5). Values over the mid-latitudes of the Northern Hemisphere showed a rising tendency from 2017 onward and peaked in summer 2018 (figure not shown). In July 2018, zonal mean temperatures in the troposphere were significantly above normal from 40 to 70°N (Figure 1.3-6). The significantly warm conditions observed are associated with the extreme heatwave seen worldwide around boreal summer (see Section 1.1).

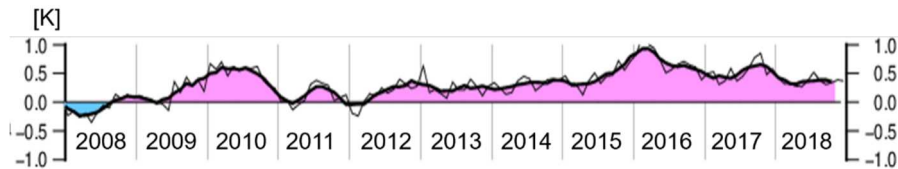


Figure 1.3-5 Time-series representation of global average temperature anomalies calculated from thickness in the troposphere (2008 to 2018)

The thin and thick lines show monthly mean and five-month running mean values, respectively. The base period for the normal is 1981 – 2010.

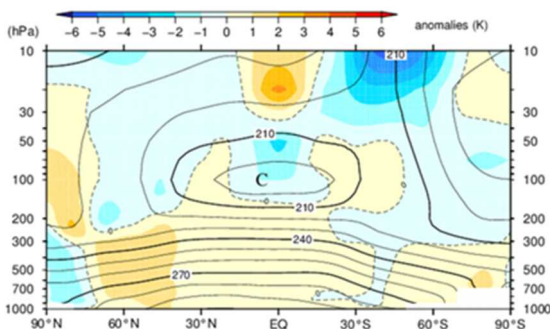


Figure 1.3-6 Latitude-height cross section of zonal mean temperature and anomaly (July 2018)

Contours show zonal mean temperature at intervals of 10 K, and shading indicates temperature anomalies. The base period for the normal is 1981 – 2010. “W” and “C” denote warm and cold conditions, respectively.

1.3.3 Asian summer monsoon

Convection during the 2018 Asian summer monsoon season (i.e., June – September) was generally enhanced from June to August as indicated by the OLR index (SAMOI (A))⁹, JMA, 1997; Figure 1.3-7), particularly over the Philippines in the first half of June and from mid-July to August, and an associated deep monsoon trough was observed. This enhancement around the Philippines was associated with the extreme summer heatwave in Japan (see Topics I). In connection with the deep monsoon trough, near-surface westerly winds in the western part of the tropical North Pacific were stronger than normal. These conditions may have contributed to the series of typhoon events observed over the northwestern Pacific.

⁹ SAMOI (A) is defined as reversed-sign area-averaged OLR anomalies normalized by its standard deviation. The area for average is enclosed by green line in the bottom of Figure 1.3-7.

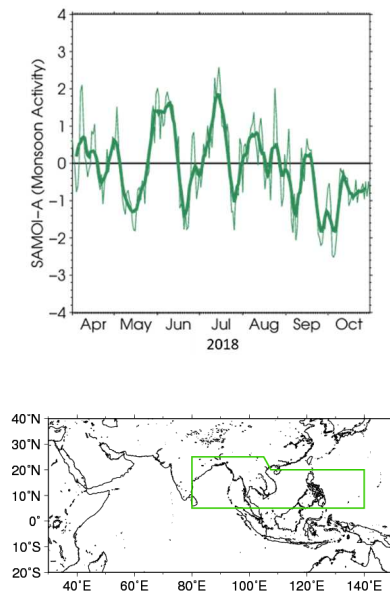


Figure 1.3-7 Time-series representation of the Asian summer monsoon OLR index (SAMOI (A)) (April – October 2018)

The thin and thick green lines indicate daily and seven-day running mean values, respectively. SAMOI (A) indicates the overall activity of the Asian summer monsoon, and positive and negative values indicate enhanced and suppressed convective activity, respectively, compared to the normal. The base period for the normal is 1981 – 2010.

1.3.4 Tropical cyclones over the western North Pacific and the South China Sea

In 2018, 29 tropical cyclones (TCs) with maximum wind speeds of ≥ 34 kt¹⁰ formed over the western North Pacific and the South China Sea (Figure 1.3-8, Table 1.3-1), which was above the normal of 25.6 (1981 – 2010 average). A total of 9 TCs formed in August 2018 (against a normal of 5.9), which tied as the third highest on record for August since 1951 behind the totals of 10 for 1960 and 1966. In addition, 7 TCs reached peak intensity with maximum wind speeds of ≥ 105 kt, which was the highest since records began in 1977 (exceeding the previous high of 6 for 1983). A total of 16 TCs came within 300 km of the Japanese archipelago, which was above the normal of 11.4. A total of 5 made landfall on Japan, exceeding the normal of 2.7.

TC Jongdari formed east of the Philippines on 24 July (JST¹¹) before moving northeastward south of the Ogasawara Islands and then westward near the Izu Islands, making landfall on the city of Ise in Mie Prefecture on 29 July (JST). This was the first TC to move westward across western Japan after making landfall since records began in 1951. TC Jebi formed around the Marshall Islands on 28 August (JST) and made landfall on the southern part of Tokushima Prefecture on 4 September (JST), making it the first TC since 1993 to make landfall on Japan with maximum wind speeds of ≥ 85 kt. Jebi brought unusually strong winds and storm surges, causing particular damage to the Shikoku and Kinki areas.

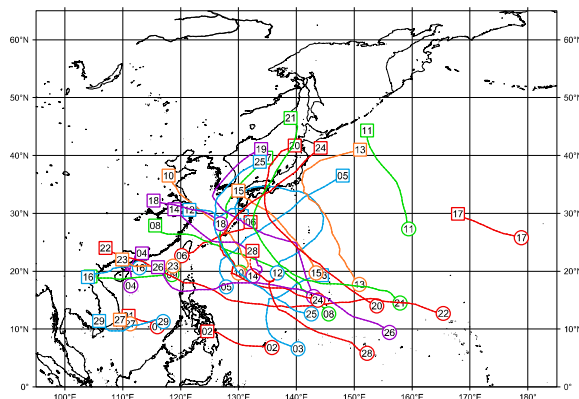


Figure 1.3-8 Tracks of TCs with maximum wind speeds of ≥ 34 kt in 2018

Numbered circles indicate positions of the TC formed (maximum wind speeds of ≥ 34 kt), and numbered squares indicate positions of the TC dissipated (maximum wind speeds lower than 34 kt). Source: RSMC Tokyo-Typhoon Center data

10 One knot (kt) is about 0.51 m/s.

11 Japan Standard Time (JST) is defined to set nine hours forward of UTC.

Table 1.3-1 TCs with maximum wind speeds of ≥ 34 kt in 2018 (Source: RSMC Tokyo-Typhoon Center data)

Number ID	Tropical Cyclone	Duration (UTC)	Maximum Wind ¹⁾ (kt)	Number ID	Tropical Cyclone	Duration (UTC)	Maximum Wind ¹⁾ (kt)
1801	BOLAVEN	1/3-1/4	35	1816	BEBINCA	8/13-8/17	45
1802	SANBA	2/11-2/13	35	1817	HECTOR	8/13-8/15	40
1803	JELAWAT	3/25-4/1	105	1818	RUMBIA	8/15-8/18	45
1804	EWINIAR	6/5-6/8	40	1819	SOULIK	8/16-8/24	85
1805	MALIKSI	6/7-6/11	60	1820	CIMARON	8/18-8/24	85
1806	GAEMI	6/15-6/17	45	1821	JEBI	8/27-9/5	105
1807	PRAPIROON	6/29-7/4	65	1822	MANGKHUT	9/7-9/17	110
1808	MARIA	7/4-7/11	105	1823	BARIJAT	9/11-9/13	40
1809	SON-TINH	7/17-7/19	40	1824	TRAMI	9/21-10/1	105
1810	AMPIL	7/18-7/23	50	1825	KONG-REY	9/29-10/6	115
1811	WUKONG	7/23-7/27	50	1826	YUTU	10/22-11/2	115
1812	JONGDARI	7/24-8/3 ²⁾	75	1827	TRAJI	11/17-11/18	35
1813	SHANSHAN	8/3-8/10	70	1828	MAN-YI	11/20-11/27 ²⁾	80
1814	YAGI	8/8-8/13	40	1829	USAGI	11/22-11/26	60
1815	LEEPI	8/11-8/15	50				

1) Estimated maximum 10-minute mean wind speed

2) The duration of Jongdari and Man-yi includes periods with maximum wind speeds intermittently lower than 34 kt.